

Supporting Information

Sandwich-type nanoporous CoO/N-doped carbon multi-layers with ultrahigh lithium storage and long-life stability

Zhaoliang Shi[†], Yuzun Fan[†], Wei Zhou, and Lin Guo*

School of Chemistry, Beijing Advanced Innovation Center for Biomedical Engineering, Beihang University, Beijing 100191, China

[†]Z.L. Shi and Y.Z. Fan contributed equally to this work.

*Corresponding author. Email: zhouwei@buaa.edu.cn.

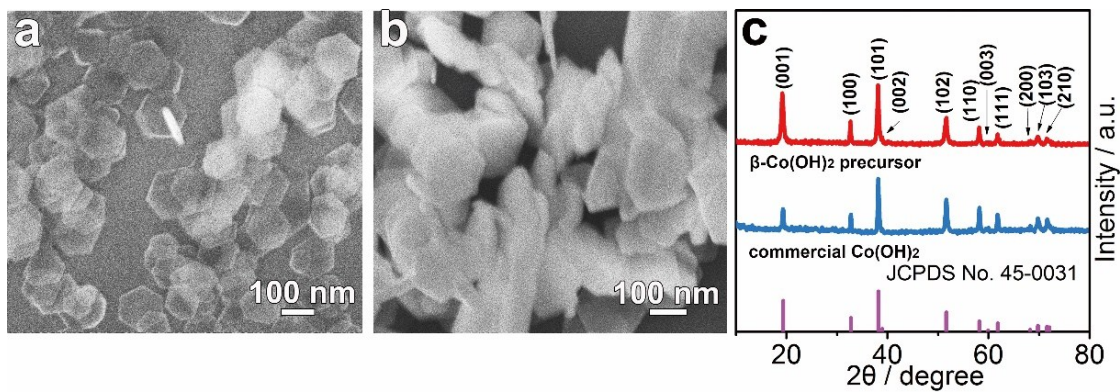


Fig. S1. SEM images of (a) the precursor of $\beta\text{-Co(OH)}_2$ hexagonal platelets with an average side length of 100 nm; (b) commercial Co(OH)_2 platelets about 100~200 nm in diameter; (c) XRD patterns of the two kinds of the precursors: $\beta\text{-Co(OH)}_2$ precursors (top) and commercial Co(OH)_2 (bottom). The diffraction peaks of these precursors are all indexed to the components of the hexagonal cell of brucite-like $\beta\text{-Co(OH)}_2$ (JCPDS No.45-0031).

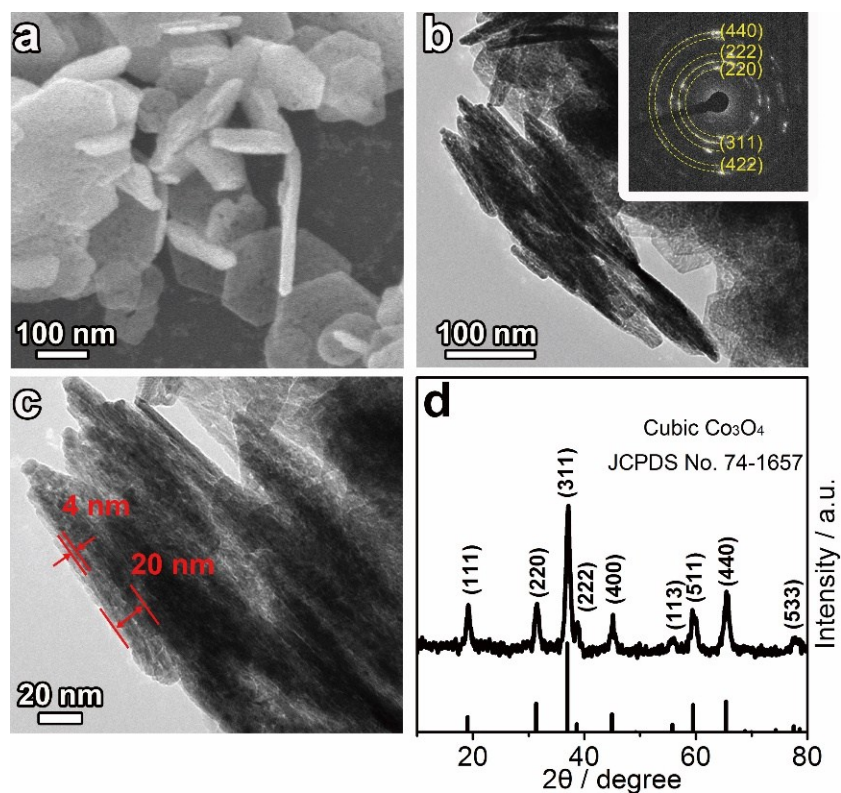


Fig. S2. (a) SEM image of the Co_3O_4 MLs with an average thickness of 20 nm obtained by annealing the precursor in air at 350 °C for 1h. (b) TEM image and SAED patterns (inset), and (c) magnified TEM image of the vertical Co_3O_4 MLs composed of several 4 nm-thick ultrathin sheets. (d) XRD patterns of the Co_3O_4 MLs. The diffraction peaks are indexed to the component of the cubic Co_3O_4 (JCPDS No.74-1657).

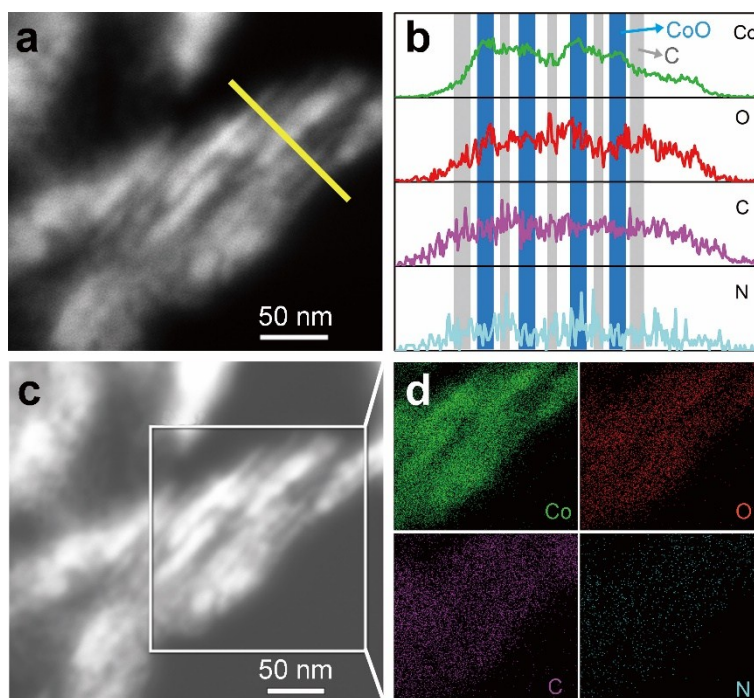


Fig. S3. (a) EDX line scan of CoO/N-C on a cross-sectional STEM image of the s-CoO/N-C ML and (b) the corresponding element distributions of Co, O, C, and N, respectively. (c) STEM images and (d) the elemental mapping of Co, O, C, and N, respectively.

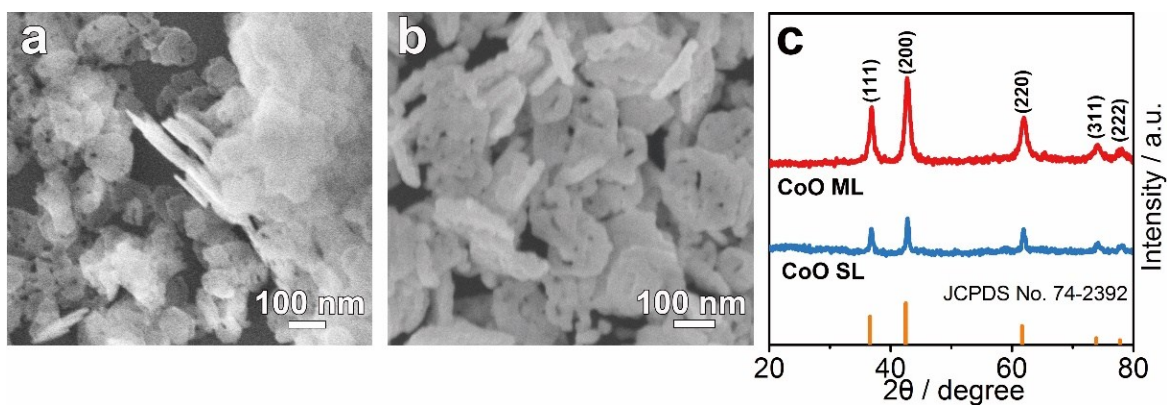


Fig. S4. (a) SEM image of CoO MLs with an average size of ~ 100 nm; (b) SEM image of CoO SLs with an average size of ~ 200 nm. As the CoO sheets are composed of aggregated particles with clear pores, which cannot be seen clear layered structure, we call the sample CoO single layers (CoO SLs). (c) XRD patterns of the CoO MLs (top) and CoO SLs (bottom). Both diffraction peaks can be indexed to the components of the cubic CoO (JCPDS No.74-2392).

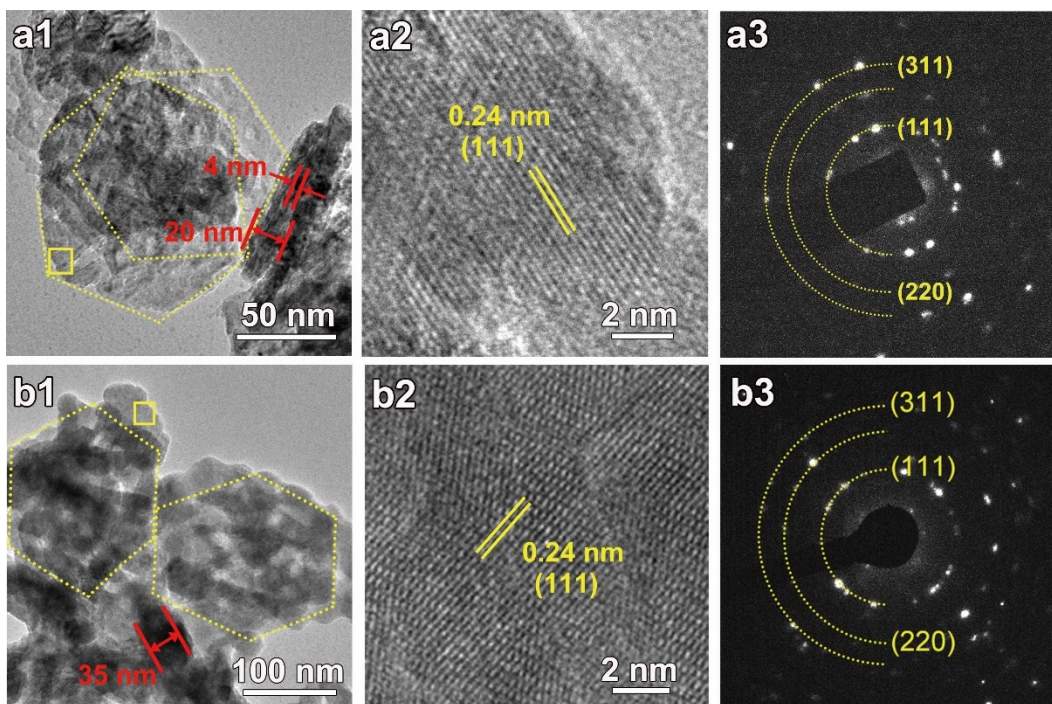


Fig. S5. TEM, HRTEM images and SAED patterns of (a1-a3) CoO MLs with a thickness of ~20 nm, composed of several 4 nm-thick ultrathin CoO sheets, and (b1-b3) porous CoO SLs with a single ~35 nm-thick sheet. The corresponding HRTEM images both show the plane of (111) of CoO. The SAED patterns confirm the CoO MLs and CoO SLs are polycrystalline.

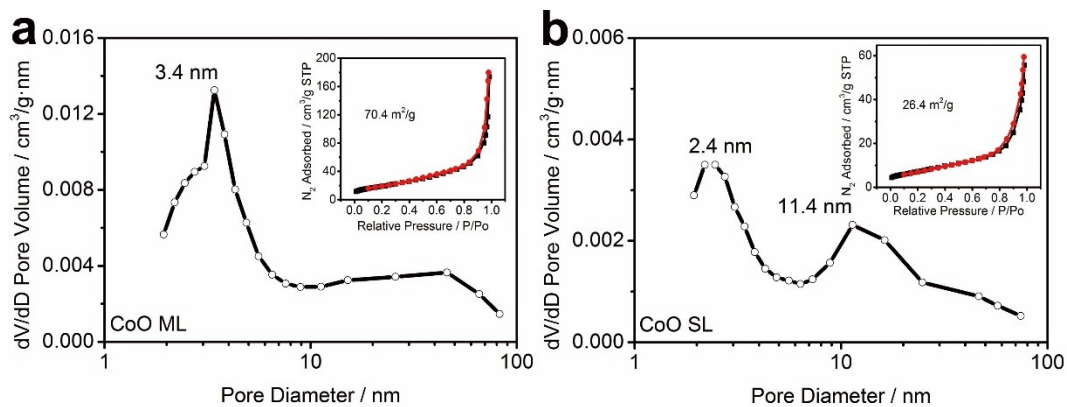


Fig. S6 Pore size distributions of (a) CoO MLs and (b) CoO SLs. The insets are the corresponding N_2 adsorption/desorption isotherms.

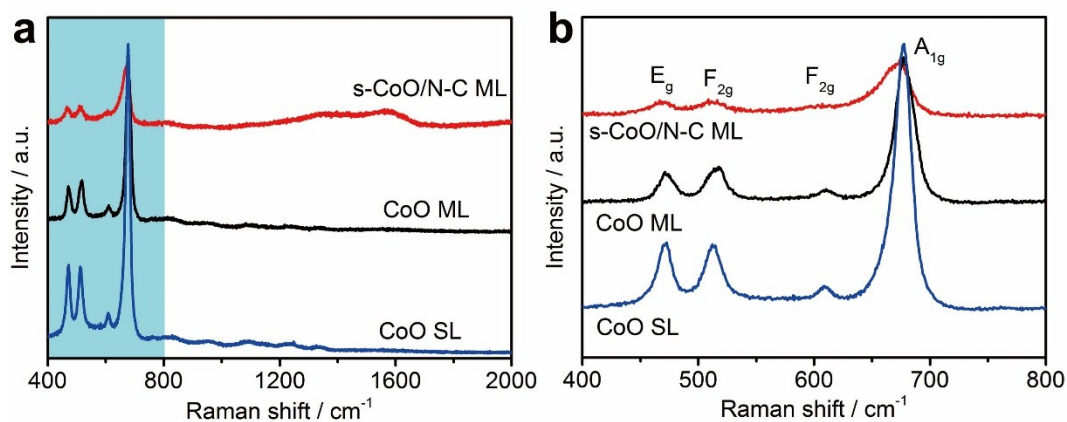


Fig. S7 (a) Raman spectra of the s-CoO/N-C MLs, CoO MLs and CoO SLs with Raman shift range of 400-2000 cm^{-1} . (b) Partial enlarged Raman spectra corresponding to the marked region in Fig. S7a.

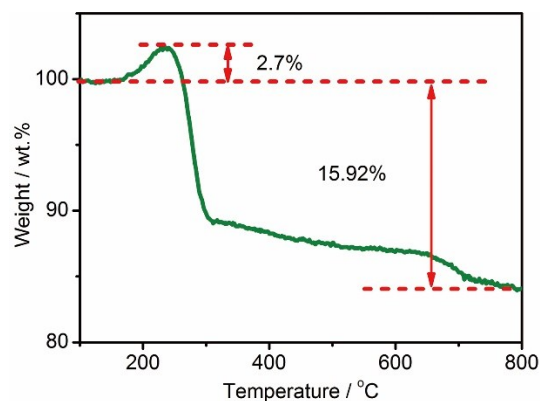


Fig. S8. TGA curve of the s-CoO/N-C MLs.

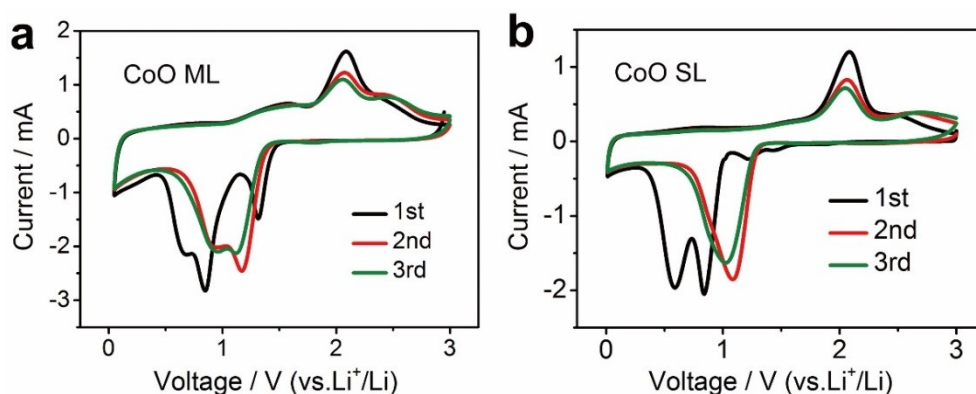


Fig. S9. CV curves of CoO MLs (a) and CoO SLs (b) for the first three cycles at 0.5 mV s^{-1} .

As shown in Fig. S9a, the CV profile of the sample displays three reduction peaks at 1.31, 0.85, and 0.66 V in the first discharging process, which can be attributed to Li^+ insertion into the sample, the conversion reaction between CoO and Li^+ to form metallic Co and Li_2O , and the formation of SEI layer on the surface of electrode material, respectively.^[S1-S5] During the subsequent cycles, the cathodic peak corresponding to the conversion of CoO to Co shifts to a higher potential due to decreased cathodic polarization. For the CoO SLs, a similar cathodic process was observed (Fig.S9b). Notably, we can observe clear peaks corresponding to Li^+ insertion in the second and third cycles in the CoO MLs, while the peak in the CoO SLs

disappears. It might be ascribed to the complex layer-by-layer structure of CoO MLs, which provides more channels for Li^+ insertion.

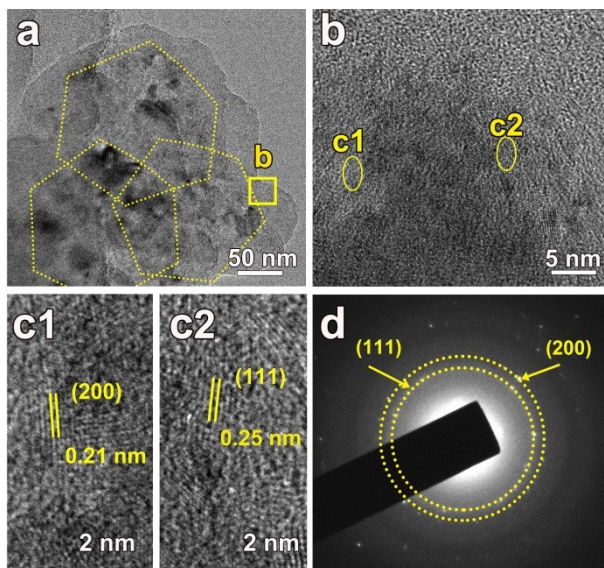


Fig. S10. (a) TEM image, (b) magnified TEM image, (c₁, c₂) HRTEM images, and SAED pattern of the s-CoO/N-C MLs after 500 cycles.

As shown in Fig. S10, the images clearly show lattice fringes of 0.21 nm and 0.25 nm, corresponding to the (200) and (111) planes of CoO, respectively, which is also consistent with the SAED patterns (Fig. S10d). These results demonstrate the Co is oxidized to CoO in electrochemical reaction.

Table S1. Comparison of rate capabilities of different Co-based materials for LIBs.

Samples	Current density (A g⁻¹)	Rate capability (mAh g⁻¹)	Reference
sandwich-type CoO/ N-doped carbon multi-layers (s-CoO/N-C MLs)	5	975.1	This work
CoO hollow cube/RGO [S1]	0.75	654	Chem. Mater., 2014
pomegranate-like CoO@N-doped carbon [S2]	2	450	J. Mater. Chem. A, 2017
hollow CoO@B, N co-doped graphitic nanotube [S3]	3	247	Adv. Mater., 2018
CoO@C arrays [S4]	4	536	Nano Energy, 2014
dense CoO/G stacks [S5]	5	297	J. Power Sources, 2014
peapod-like Co ₃ O ₄ @carbon nanotube arrays [S6]	5	408	Angew. Chem. Int. Ed., 2015
CoO@C dandelions [S7]	5	400	Adv. Energy Mater., 2018
triple-shelled Co ₃ O ₄ @Co ₃ V ₂ O ₈ nanoboxes [S8]	5	550	Adv. Mater., 2018

Table S2. Comparison of cycling performance of different Co-based materials for LIBs.

Samples	Current density(A g⁻¹)	Cycle number	Capacity (mAh g⁻¹)	Reference
sandwich-type CoO/N-doped carbon multi-layers (s-CoO/N-C MLs)	0.5	500	1031.2	This work
	1	1200	864.8	
	10	1200	538.8	
CoO@C dandelions [S7]	0.5	300	840	Adv. Energy Mater., 2018
triple-shelled Co ₃ O ₄ @Co ₃ V ₂ O ₈ nanoboxes [S8]	0.5	500	706	Adv. Mater., 2018
starfish-like Co ₃ O ₄ @N-C [S9]	0.5	300	795	Nano Res., 2017
carbon-doped Co ₃ O ₄ nanocrystals [S10]	0.5	300	950	Adv. Funct. Mater., 2018
hierarchical CNT/Co ₃ O ₄ microtubes [S11]	1	200	782	Angew. Chem. Int. Ed., 2016
foam-like CoO@N,S co-doped carbon [S12]	1	500	809	J. Mater. Chem. A, 2017
Co ₃ O ₄ /C-N nanospheres [S13]	1	500	798	J. Mater. Chem. A, 2018

References

- [S1] X. Guan, J. Nai, Y. Zhang, P. Wang, J. Yang, L. Zheng, J. Zhang and L. Guo, *Chem. Mater.*, 2014, **26**, 5958-5964.
- [S2] G. Liu and J. Shao, *J. Mater. Chem. A*, 2017, **5**, 9801-9806.
- [S3] H. Tabassum, R. Zou, A. Mahmood, Z. Liang, Q. Wang, H. Zhang, S. Gao, C. Qu, W. Guo and S. Guo, *Adv. Mater.*, 2018, **30**, 1705441.
- [S4] J. Liu, Y. Xu, X. Ma, J. Feng, Y. Qian and S. Xiong, *Nano Energy*, 2014, **7**, 52-62.
- [S5] S. J. R. Prabakar, R. S. Babu, M. Oh, M. S. Lah, S. C. Han, J. Jeong and M. Pyo, *J. Power Sources*, 2014, **272**, 1037-1045.
- [S6] D. Gu, W. Li, F. Wang, H. Bongard, B. Spliethoff, W. Schmidt, C. Weidenthaler, Y. Xia, D. Zhao and F. Schuth, *Angew. Chem. Int. Ed.*, 2015, **54**, 7060-7064.
- [S7] F. Wu, S. Zhang, B. Xi, Z. Feng, D. Sun, X. Ma, J. Zhang, J. Feng and S. Xiong, *Adv. Energy Mater.*, 2018, **8**, 1703242.
- [S8] Y. Lu, L. Yu, M. Wu, Y. Wang and X.W. Lou, *Adv. Mater.*, 2018, **30**, 1702875.
- [S9] Y. Sun, F. Huang, S. Li, Y. Shen and A. Xie, *Nano Res.*, 2017, **10**, 3457-3467.
- [S10] C. Yan, Y. Zhu, Y. Li, Z. Fang, L. Peng, X. Zhou, G. Chen and G. Yu, *Adv. Funct. Mater.*, 2018, **28**, 1705951.
- [S11] Y. M. Chen, L. Yu and X. W. Lou, *Angew. Chem. Int. Ed.*, 2016, **55**, 5990-5993.
- [S12] F. Wang, H.-Y. Zhuo, X.Han, W.-M. Chen and D. Sun, *J. Mater. Chem. A*, 2017, **5**, 22964-22969.
- [S13] H. Xue, Z. Na, Y. Wu, X. Wang, Q. Li, F. Liang, D. Yin, L. Wang and J. Ming, *J. Mater. Chem. A*, 2018, **6**, 12466-12474.